PHYSICAL REVIEW E **87**, 012308 (2013)

Nucleation and growth of thermoreversible polymer gels

J. R. Gomez-Solano, V. Blickle, and C. Bechinger
2. Physikalisches Institut, Universität Stuttgart, Pfaffenwaldring 57, 70569 Stuttgart, Germany and
Max-Planck-Institute for Intelligent Systems, Heisenbergstrasse 3, 70569 Stuttgart, Germany
(Received 30 August 2012; published 14 January 2013)

We study the spatiotemporal low-frequency microrheology of a gelatin gel during the sol-gel transition after a fast temperature quench by tracking the motion of embedded colloidal particles. From the particle dynamics two different mechanisms responsible for the gelation of the sol phase can be identified: a fast process associated to the local nucleation of triple helices and a slow fiber growth triggered by presence of an intact network. We associate the latter to a gelation front propagating into the sol phase whose speed depends linearly on the quench depth and which accelerates the local rate of the sol-gel transition.

DOI: 10.1103/PhysRevE.87.012308 PACS number(s): 82.70.Gg, 83.80.Kn, 87.15.Zg

I. INTRODUCTION

Physical gelation is a common process that occurs in numerous soft materials such as biopolymers, block copolymers, liquid crystals, colloid-polymer mixtures, and micellar solutions [1,2]. A viscoelastic gel phase is formed by a network of low-volume fraction, being stabilized by reversible bonds that develop within an initially liquid-like phase (sol). Recent experiments and simulations show that different mechanisms, depending on the microscopic gel structure, are involved during the development of such a network: e.g., arrested spinodal decomposition [3], diffusion-limited cluster aggregation [4], jamming [5], and fiber growth [6]. This suggests that, unlike chemical gelation, where the formation of irreversible bonds is described in terms of a connectivity transition within the Flory-Stockmayer percolation theory [7], physical sol-gel transitions are considerably more complex. Therefore, a better understanding of the physical mechanisms leading to reversible gel networks and of the dynamical properties of the pre-gel state is important in the context of soft matter phase transitions.

In particular, *thermoreversible* polymer gels have attracted much attention since their physical properties can be easily controlled by temperature. By decreasing the temperature below the gelation temperature $T_{\rm gel}$, the arrest is due to the frustration of compact molecular structures (helices, crystallites) that are interconnected by reversible bonds (cross links) [2]. This leads to a slow time evolution of their structural and mechanical properties (physical aging) whose dynamics depends on the specific temperature protocol and the fraction of bonds. In particular, the bulk rheology of aqueous gelatin solutions has been extensively studied as an experimental model system of thermoreversible polymer gels [1,8,9]. Despite numerous macroscopic studies on thermoreversible polymer gels, only a few investigated the microscopic details of network formation in the pre-gel phase [10–13]. Some of these results stress the importance of a spatially heterogeneous dynamics during the formation of the gel network [11–13].

In the present work, we study the low-frequency microrheology of a gelatin gel that has been locally liquefied by laser heating and then quenched below the gelation temperature. We provide experimental evidence that in addition to the well-known network formation by the homogeneous nucleation of triple helices [1], a gelation front starts from the intact gel at the edge of the heated area and propagates into the aging sol phase, thereby increasing the gelation rate. With our experimental setup, we are able to clearly distinguish between these processes. Our results suggest that in the presence of interfaces, network formation can be significantly accelerated by heterogeneous processes.

II. EXPERIMENT

The experimental setup is shown in Fig. 1(a). It consists of a thin layer ($h = 4\,\mu$m) of a thermoreversible biopolymer gel (bovine skin gelatin at 10% wt in water) confined between two glass plates. At this concentration and above $T_{\rm gel} = 28 \pm 0.5^\circ$ [14], the gelatin chains have a random single-stranded coil conformation that results in a homogeneous sol phase. Below $T_{\rm gel}$, the gel phase is induced by the formation of triple helices stabilized by hydrogen bonds. The sample cell is kept at constant temperature $T_0 < T_{\rm gel}$ using a thermostat. The sample contains a small volume fraction of red-fluorescent microspheres (diameter $2a = 0.5\,\mu$m) used as tracers in order to probe the microrheology of the system. An infrared laser beam (Raman Fiber, $\lambda = 1455$ nm) is weakly focused into the sample where it liquefies the gel within a cylindrical region with radius $R = 25\,\mu$m due to light absorption of water. A typical temperature profile, determined by Rhodamine dye (TAMRA dissolved in Tris-HCL buffer solution), for a bath temperature $T_0 = 20^\circ$C and a laser exposure over 30 s of 400 mW is shown in Fig. 1(b). Within such long exposure times, we guarantee that the gel is completely liquefied and a steady state is obtained. To demonstrate the response of the tracers to such a temperature profile, we also show some trajectories in Fig. 1(b). Within the liquefied region, where $T > T_{\rm gel}$, the particle's mobility is much larger compared to those areas at $T < T_{\rm gel}$, where the particle's motion is constrained by the elastic gel matrix. The observed radial particle drift results from the thermophoretic motion of the tracers driven by the temperature gradient during the melting process of the gel.

In our experiments, we study the gelation process of the laser-induced initial sol phase which is surrounded by an intact gel matrix. After turning off the laser power, the temperature distribution within the sample becomes uniform and equal to the bath temperature T_0 by heat diffusion into the bulk within $\lesssim$10 ms. The main control parameter is the *quench depth*,

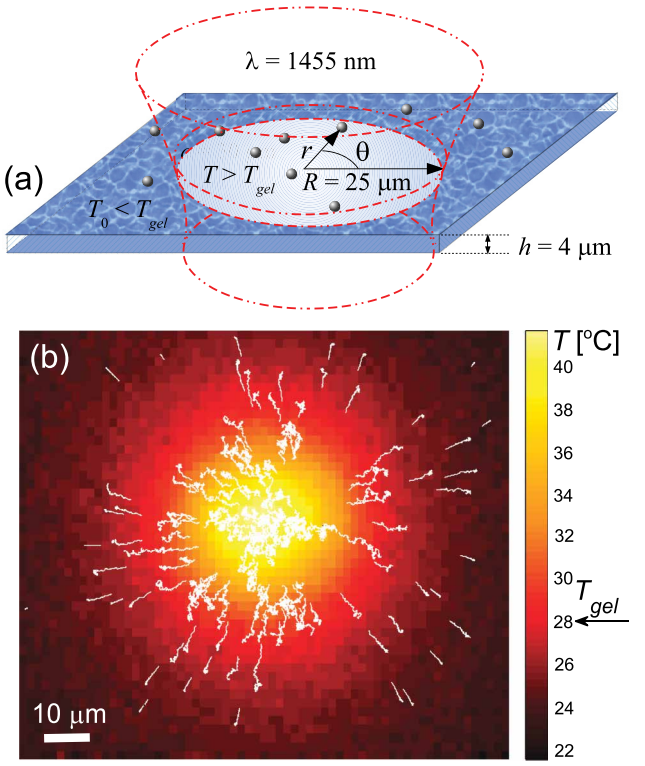

FIG. 1. (Color online) (a) Sketch of the experimental setup where a cylindrical region of a gel is liquefied by a laser beam (dot-dashed lines). (b) Temperature profile within the sample created by the laser beam. Examples of trajectories of colloidal tracer particles during the melting process of the gel (solid white lines).

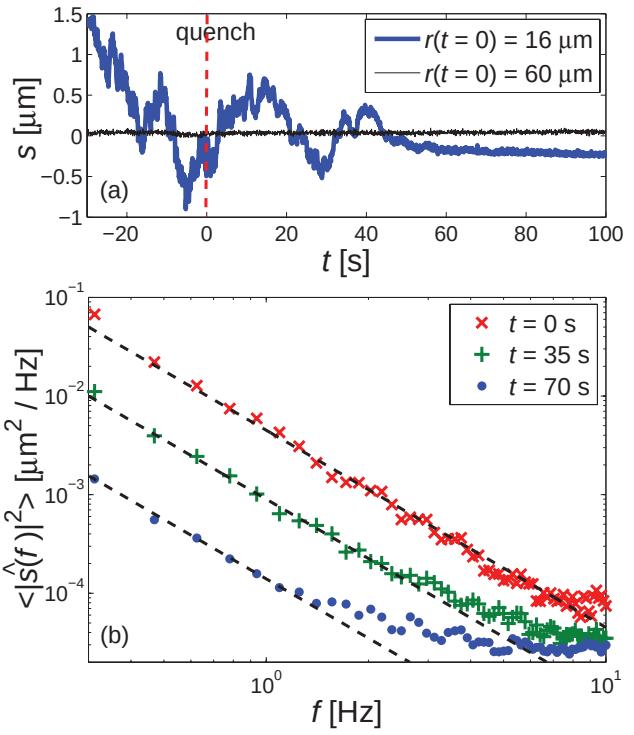

FIG. 2. (Color online) (a) Examples of trajectories $s(t)$ of a colloidal tracer located inside the liquefied region (thick blue line) and one in the gel matrix (thin black line) at time $t = 0$. (b) Power spectral density of $s(t,\Delta t,r,\Delta r)$ computed over $[r = 0,\Delta r]$ and the time interval $[t,t+\Delta t]$ at different times t after the quench. The black dashed lines are fits according to Eq. (1) on the low-frequency range of the spectra.

defined as $\Delta T = T_{\rm gel} - T_0$. In this way we are able to probe the initial stage of gelation after the quench at $T = T_0$ by video microscopy of the tracers (sampling frequency 20 Hz, spatial resolution 25 nm). Due to the circular geometry imposed by the laser spot, the tracer's trajectories are analyzed in polar coordinates (r,θ) centered relative to the maximum of the temperature distribution during the melting process, as depicted in Fig. 1(a). By analyzing the time-dependent radial component $r(t)$ of the tracer trajectories, we found that after turning off the laser, the thermal contraction of the gel due to the temperature quench takes place within ≈100 ms. After this transient regime, which is much shorter than the typical gel aging time, thermophoresis of the tracers and thermal contraction of the gel can be completely disregarded. Because in the following we are only interested in the gelation dynamics, the time $t = 0$ s is defined as 100 ms after the laser has been turned off.

Due to the isotropy in the angular direction, we restrict our analysis to the angular component of the particle trajectories $s(t) = \int_{0\,\rm s}^{t} r(t')\dot{\theta}(t')\,{\rm d}t'$. In Fig. 2(a) we show exemplarily a trajectory of a tracer at $r(t = 0) = 16\,\mu$m, i.e., inside the liquefied region during the quench. After the heating laser is turned off, the fluctuations decrease due to the increasing elasticity of the forming network. For comparison, we also plot the trajectory of a particle located far from the center of the heating spot $[r(t = 0) = 60\,\mu$m], which is always confined by the already formed network. To characterize the microrheology of the aging sol phase, from the particle trajectories we compute its local zero-shear (micro-)viscosity η_0 as a function of the time t elapsed after the quench and the radial distance r from the origin of the polar coordinate system. In order to consider trajectories where $r \approx$ const., we divide them into segments that do not exceed the radial distance $[r, r+\Delta r]$ within the time interval $[t, t+\Delta t]$. For the calculation of the proper averages, we set the values of the spatial and temporal binning to $\Delta r = 5\,\mu$m and $\Delta t = 5$ s. Finally, for each trajectory segment $s(t,\Delta t,r,\Delta r)$ we compute its Fourier transform $\hat{s}(f)$ over the frequency range $0.03\ {\rm Hz} < f \leqslant 10$ Hz. By averaging over typically 200 quenching protocols, we obtain the power spectral density $\langle|\hat{s}(f)|^2\rangle$ of the angular particle fluctuations, which is shown as symbols in Fig. 2(b) for $r = 0\,\mu$m and $t = 0$ s, 35 s, 70 s. From the low-frequency range, the particle diffusivity $D_s(t,r)$ is determined from

$$\langle|\hat{s}(f)|^2\rangle = \frac{D_s(t,r)}{\pi^2 f^2}, \tag{1}$$

which is shown by dashed lines in Fig. 2(b). The deviations between the experimental data and the fit according to Eq. (1) at high frequencies are due to the increasing elasticity of the developing network. Using the Stokes-Einstein relation, we then obtain the zero-shear viscosity, which now depends on the time and the radial distance:

$$\eta_0(t,r) = \frac{k_B T_0}{6\pi a D_s(t,r)}. \tag{2}$$

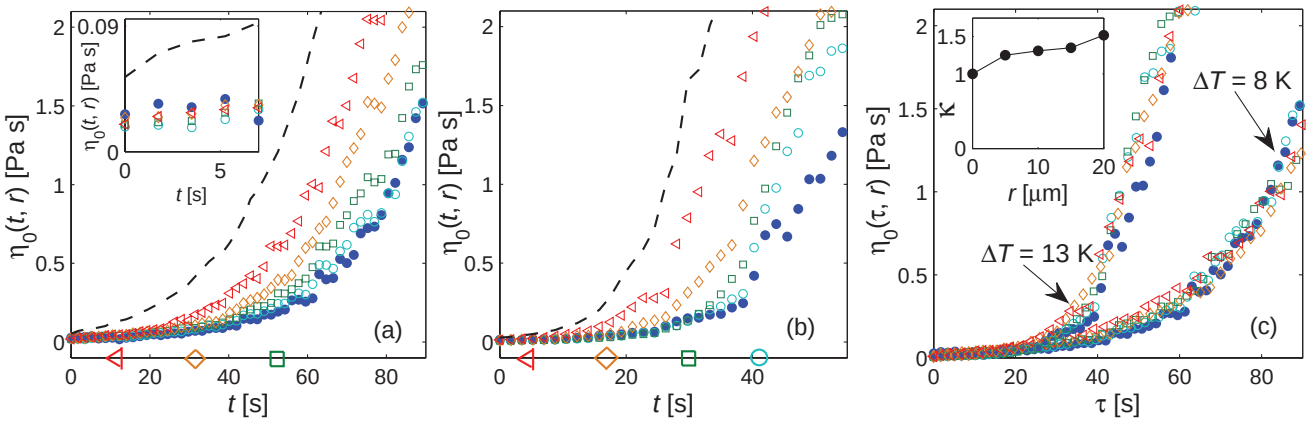

FIG. 3. (Color online) Time evolution of η_0 for 10% wt gelatin concentration in water after the quench for (a) $\Delta T = 8$ K and (b) $\Delta T = 13$ K at different radial distances: $r = 0\,\mu$m (•), $5\,\mu$m (○), $10\,\mu$m (□), $15\,\mu$m (◇), $20\,\mu$m (◁). The dashed line corresponds to $r = 30\,\mu$m. The symbols on the horizontal axis indicate the location of the time t_f defined by Eq. (3) used to compute the front speed. Inset: expanded view of η_0 at short times after the quench. (c) Zero-shear viscosity as a function of the aging time rescaled according to Eq. (4) for $\Delta T = 8$ K and $\Delta T = 13$ K. Same symbols as in (a) and (b). Inset: radial dependence of the parameter $\kappa(r)$ defined by the rescaling relation (4) for $\Delta T = 13$ K.

Although Eq. (2) is strictly applicable only close to thermal equilibrium, the relation is also valid to probe the thermal motion of the gelatin chains in our experiments because the time interval $\Delta t = 5$ s is much smaller compared to the aging time of the system. The time evolution of η_0 for different values of r and for two quench depths $\Delta T = 8$ K and $\Delta T = 13$ K, is plotted in Figs. 3(a) and 3(b), respectively. During the illumination and melting of the sample, the viscosity of the liquefied region of the sample is not uniform due to the temperature dependence of η_0 (data not shown). Immediately after the quench, η_0 becomes constant across the entire liquefied region as shown in the inset of Fig. 3(a). This proves that the temperature becomes uniform below our temporal resolution after switching off the laser. In contrast, at larger distances where $T < T_{\rm gel}$ for $t < 0$ s ($r = 30\,\mu$m, dashed line) the viscosity slowly increases for $t > 0$ s, which is consistent with the rheological behavior of preaged gels obtained from bulk rheological measurements [9].

III. RESULTS AND DISCUSSION

We now focus on the long-time rheological properties after the quench. Since the system is not in equilibrium at $t = 0$, η_0 increases for $t > 0$. This increase, which is observed over the entire sample, suggests the development of a gel network by an increasing number of locally cross-linked triple-helices [Fig. 3(a)]. A similar behavior is also found when the quench depth is increased to $\Delta T = 13$ K [Fig. 3(b)]. However, it should be noted that with increasing quench depth, the increase of η_0 becomes faster. This is consistent with bulk measurements where the triple-helix formation was found to be enhanced at lower temperatures [8]. In addition to an overall increase of η_0 with ΔT from our measurements we observe a pronounced increase of the aging with increasing radial distance r. Because this spatial dependence is observed within the region that was entirely liquefied by the laser beam, our observation suggests that the presence of a surrounding intact network can affect the gelation of the enclosed sol. Since the rheological behavior of gelatin below $T_{\rm gel}$ is only determined by the fraction of triple helices in the solvent [9], the spatiotemporal variation of η_0 must be due to the propagation of a *gelation front* of triple helices from the surrounding gel into the sol phase.

In order to characterize the dynamics of this gelation front, we determine the time t_f at which the evolution of the curve $\eta_0(t,r)$ first deviates from that of the central curve $\eta_0(t,r = 0)$ by an amount $0.2\eta_0$, equal to the statistical error of the computation of η_0, i.e.,

$$t_f = \min\{t : \eta_0(t,r) \geqslant \eta_0(t,0) + 0.2\eta_0\}. \tag{3}$$

The values of t_f for each r are marked by the corresponding symbols on the horizontal axis of Figs. 3(a) and 3(b). We chose $\eta_0(t,r = 0)$ as the reference curve because at $r = 0$ the dynamics is the latest affected by the front motion. Interestingly, for $t > t_f$, the viscosity increases considerably faster with increasing r. Despite the apparently complex spatial and temporal viscosity dependence during the gelation process, *all* data collapse to $\eta_0(t,r = 0)$ by using a simple rescaling relation:

$$\tau(r) = \begin{cases} t & t < t_f(r) \\ t_f(r) + \kappa(r)[t - t_f(r)] & t \geqslant t_f(r). \end{cases} \tag{4}$$

This is shown in Fig. 3(c) for $\Delta T = 8$ K and $\Delta T = 13$ K. The parameter $\kappa(r)$ is introduced in order to quantify the rate at which the gelation front accelerates the aging dynamics of the sol phase at a given position r with respect to the center. The values of $\kappa(r)$, which are exemplarily shown for $\Delta T = 13$ K in the inset of Fig. 3(c), are always larger than or equal to one. Despite the nonlinear dependence of $\kappa(r)$, it should be realized that it does not alter the qualitative gelation dynamics because it only enters linearly in Eq. (4). Its monotonically increasing dependence on r is consistent with both the local nucleation of triple-helices and the front propagation from the intact network. Indeed, for short t, there are many triple-helices available to form the fiber network by the front-induced mechanism; therefore, $\kappa(r) > 1$ must be large for large r. As the front propagates and arrives to a smaller r, the system has

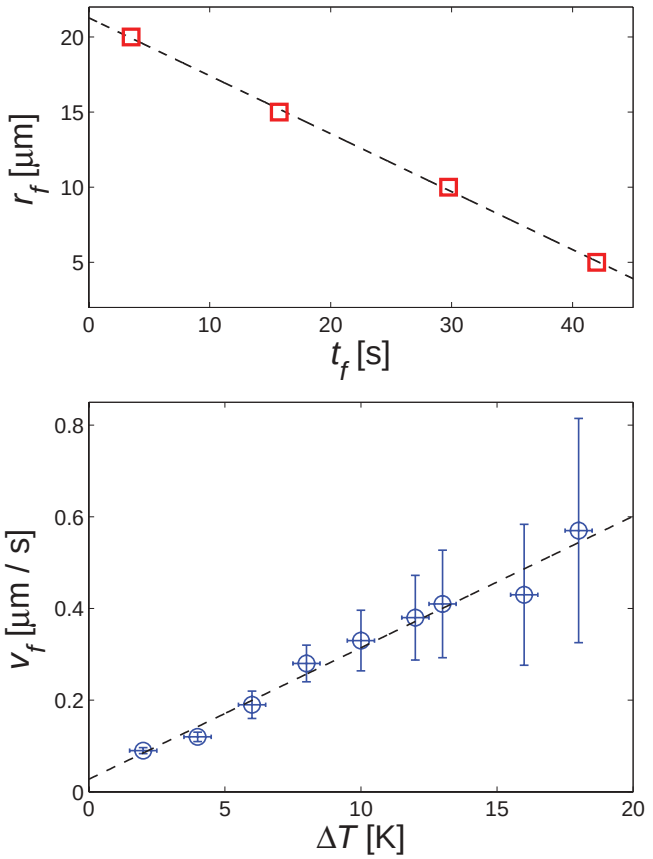

FIG. 4. (Color online) (a) Time evolution of the radial position r_f of the gelation front for $\Delta T = 13$ K. (b) Front velocity as a function of the quench depth. The dashed line represents the best linear fit of the experimental data (circles).

already developed a weak network at that position so that the amount of available triple-helices to be affected by the front motion is smaller.

To understand how the gelation front propagates into the sol, we plotted its position r_f at time t_f in Fig. 4(a) for $\Delta T = 13$ K. The linear dependence suggests that the gelation front propagates at a constant speed of $v_f = 0.4\,\mu\mathrm{m\,s}^{-1}$. We measured the front speed for different values of the quench depth. In Fig. 4(b) we plot the results. The relation between v_f and ΔT turns out to be linear: $v_f \sim \Delta T$ [see the linear fit in Fig. 4(b)]. As expected, the front speed becomes zero at $T_0 = T_{\mathrm{gel}}$, since at this temperature there is no network in the bulk that can propagate into the sol phase to induce its gelation.

The observation of a gelation front propagating toward the liquefied region can be interpreted as the heterogeneous nucleation and subsequent growth of triple helix fibers. Obviously, the reorganization of helices into fibers is started at the boundary of the surrounding gel network from where the network grows with constant speed. This interpretation is consistent with recent experiments where the fiber aggregation of triple helices was identified as an important mechanism for the development of a network in gelatin gels [15]. In addition, indirect evidence for a propagating gelation front was obtained from nonthermal forces acting on a colloidal probe during the sol-gel transition after a temperature quench [16]. Consequently, our results support that gelation of thermoreversible polymer gels can be regarded as a two-step aggregation phenomenon. First, compact molecular structures (triple-helices in the present case) nucleate within the sol, which, secondly, aggregate into fiber structures [15,17], thus suggesting a qualitative resemblance to colloidal gelation [3,18,19] and colloidal crystallization [20,21]. Our results should be applicable to a broad class of polymer gels where the formation of the network proceeds via connection of compact molecular structures that must first nucleate, e.g., helices in agarose, carrageenans, and gellan gum; crystallites in poly(vinyl chloride) gels; and block domains in triblock copolymers [2,22].

IV. CONCLUDING REMARKS

In summary, we have studied the gelation of a microscopic sample of gelatin as a model system of a thermoreversible polymer gel in the sol phase quenched below the gelation temperature. We found that, in addition to the overall gelation process of the sol phase by local cross-linking of triple helices, a gelation front starts from the intact gel at the edge of the heated area and propagates into the aging sol phase, thereby increasing the gelation rate. We suggest that this behavior can be interpreted in terms of heterogeneous nucleation and subsequent growth of triple-helix fibers.

ACKNOWLEDGMENT

We acknowledge Klaus Kroy for helpful discussions.

[1] K. T. Nijenhuis, Adv. Polym. Sci. **130**, 194 (1997).
[2] K. T. Nijenhuis, Polymer Bulletin **58**, 27 (2007).
[3] S. Manley, H. M. Wyss, K. Miyazaki, J. C. Conrad, V. Trappe, L. J. Kaufman, D. R. Reichman, and D. A. Weitz, Phys. Rev. Lett. **95**, 238302 (2005).
[4] E. H. A. de Hoog, W. K. Kegel, A. van Blaaderen, and H. N. W. Lekkerkerker, Phys. Rev. E **64**, 021407 (2001).
[5] V. Trappe, V. Prasad, L. Cipelletti, P. N. Segre, and D. A. Weitz, Nature (London) **411**, 772 (2001).
[6] J. F. Douglas, Langmuir **25**, 8386 (2009).
[7] P. J. Flory, J. Am. Chem. Soc. **63**, 3083 (1941); W. H. Stockmayer, J. Chem. Phys. **11**, 45 (1943).
[8] M. Djabourov, J. Leblond, and P. Papon, J. Phys. France **49**, 319 (1988).
[9] M. Djabourov, J. Leblond, and P. Papon, J. Phys. France **49**, 333 (1988).
[10] T. H. Larsen and E. M. Furst, Phys. Rev. Lett. **100**, 146001 (2008).
[11] A. M. Corrigan and A. M. Donald, Eur. Phys. J. E **28**, 457 (2009).
[12] D. van den Ende, E. H. Purnomo, M. H. G. Duits, W. Richtering, and F. Mugele, Phys. Rev. E **81**, 011404 (2010).
[13] R. Colin, A. M. Alsayed, J.-C. Castaing, R. Goyal, L. Hough, and B. Abou, Soft Matter **7**, 4504 (2011).

[14] H. B. Bohidar and S. S. Jena, J. Chem. Phys. **98**, 8970 (1993).
[15] D. Pelc, S. Marion, M. Pozek, and M. Basletic, arXiv:1207.4896v1.
[16] J. R. Gomez-Solano, A. Petrosyan, and S. Ciliberto, Phys. Rev. Lett. **106**, 200602 (2011).
[17] C.-M. Chou and P.-D. Hong, Macromolecules **43**, 10621 (2010).
[18] P. Lu E. Zaccarelli, F. Ciulla, A. B. Schofield, F. Sciortino, and D. A. Weitz, Nature (London) **453**, 499 (2008)
[19] A. Fortini, E. Sanz, and M. Dijkstra, Phys. Rev. E **78**, 041402 (2008).
[20] J. R. Savage and A. D. Dinsmore, Phys. Rev. Lett. **102**, 198302 (2009).
[21] M. Franke, A. Lederer, and H. J. Schöpe, Soft Matter **7**, 11267 (2011).
[22] P. Skrzeszewska *et al.*, Soft Matter **5**, 2057 (2009).